Chemical modelling of Delayed Ettringite Formation for assessment of affected concrete structures

Alain Sellier, Stéphane Multon

Chemical modelling of Delayed Ettringite Formation for assessment of affected concrete structures

Alain Sellier [(1)(2)], Stéphane Multon [(1)]

(1) LMDC, INSA/UPS Génie Civil, 135 Avenue de Rangueil, 31077 Toulouse, cedex 04 France.

(2) Corresponding author : alain.sellier@insa-toulouse.fr

Abstract

Delayed Ettringite Formation (DEF) modelling is addressed in the context of structural analysis. First, a chemical model is specified to simulate the effects of the heating of concrete in terms of reactions involving sulfates, aluminates and alkalis. It can be decomposed into: dissolution of primary sulfoaluminates at high temperature, fixation of aluminates in hydrogarnet or carboaluminates, and formation of delayed ettringite at low temperature. The influences of alkalis, temperature and water saturation on these reactions are taken into account. The main result of this model is the amount of delayed ettringite. The parameters of the proposed chemical model are fitted on a large number of experiments taken from the literature. The chemical model is then coupled with a nonlinear mechanical model based on poro-mechanics modelling. An application of chemo-mechanical coupling shows the features and benefits of such modelling to help practitioners in the management of structures affected by DEF.

Keywords: DEF, concrete, finite element, modelling

Introduction

Unexpected combinations of cement composition and curing conditions can lead to Delayed Ettringite Formation (DEF). This well-known deleterious chemical reaction takes place in the cement matrix often several years or decades after the concrete has been heated sufficiently to dissolve primary sulfoaluminate hydrates. The main causes of excessive heating can be either the exothermic reactions of cement hydration (which can occur particularly in massive structures like dams, large foundations, columns or beams), or overheating during the production of precast concrete elements. Since recommendations became available concerning the prevention of this problem (limits on the maximum temperature during hydration and of the amount of sulfates and alkali in cement), concrete structures can be built without apprehension [21]. However, the aptitude of DEF-affected structures has to be assessed to manage potential repairs or replacement. Various tools are available to help practitioners in this choice: follow-up of cracking to observe damage induced by the DEF, laboratory analysis, and residual swelling tests on core samples are the most used [28]. These experimental techniques are performed at a given moment and location. The question of the residual strength of the whole structure, and the future evolution of damage in the structure can only be addressed by combining these techniques with modelling. Unfortunately, DEF depends on many parameters (cement chemistry, interaction with aggregates, possibility of alkali leaching, concrete porosity, strength, concrete mechanical behaviour, maximum temperature reached, duration of the hot periods, water saturation, stress and strain states, and damage), so designing a DEF model applicable at the structure scale remains a challenge. Some models based on thermodynamic considerations are already able to explain the different reactions leading to DEF [19,36]. They are highly nonlinear, as several coupled equations have to be solved simultaneously, and are thus difficult to use in the context of structural analysis in an industrial situation where several thousands of chemical and structural computation have to be performed simultaneously at each node of finite element meshes and at each step of stepwise analysis. From a mechanical point of view, efficient nonlinear models exist to analyse structural behaviour affected by swelling problems [10,23,25,37,38] but they are not yet able to consider all the chemical particularities of DEF. The purpose of this work is to propose a simplified chemical model answering the need for structural modelling. It has to be simple enough to be coupled with a nonlinear mechanical model implementable in a finite element code. The paper starts with the chemical model assumptions and equations, and this model is then fitted on a large number of experiments from the literature. Finally, the chemical model coupled with the nonlinear mechanical model based on poro-mechanics

considerations is used to analyse the development of DEF expansion and cracking in a concrete cylinder. The features and the interest of a coupled chemo-mechanics approach to managing concrete structures affected by DEF is thus illustrated.

1 Principles and notations

In this model, the mineralogy of concrete is idealized in main phases noted E_1 and M_1 respectively for the number of moles of primary ettringite and of primary monosulfate per unit of concrete volume. These primary hydrates correspond to the theoretical amount that would be created in standard conditions (ambient temperature, high humidity, complete hydration of cement). Their initial values can be computed from the amount of cement, the chemistry of which is usually supplied by the cement manufacturer. The number of moles of delayed ettringite is noted E_2. It corresponds to the amount of delayed products created after a thermal cycle causing a dissolution of primary species. Assessing these products is the aim of the present chemical model. Sulfates and aluminates adsorbed in C-S-H during the heating period are considered to be available for DEF if the required environmental conditions occur. They are noted $\tilde{S}$ and $\tilde{A}$ in the mass balance equations. The correspondence between the variables, the chemical notations and the usual cementitious abbreviations is given in Table 1.

Table 1 : Notation correspondence between model abbreviation, cementitious notation and general chemistry notation

Name / Notation (mole)	Model	Cementitious	General Chemistry Notation
Anhydrous phases			
Tricalcium Aluminate	C_3A	C_3A	$(CaO)_3(Al_2O_3)$
Ferrite	C_4AF	C_4AF	$(Ca0)_4(Al_2O_3)(Fe_2O_3)$
Equivalent Tricalcium Aluminate	C_3A^{eq}	$C_3A + 2C_4AF$	$(CaO)_3(Al_2O_3) + 2(Ca0)_4(Al_2O_3)(Fe_2O_3)$
Gypsum	$C\bar{S}$	$C\bar{S}$	$(Ca0)(SO_3)$
Water	H	H	H_20
Equivalent Alkali	Na_2O^{eq}	Na_2O^{eq}	$Na_2O + 0.658\ K_2O^{(1)}$
Hydrates and Ions (free or absorbed)			
Ettringite	E_1, E_2	$(C_3A)(C\bar{S})_3H_{32}$	$(CaO)_6(Al2O3)(SO3)_3 \cdot 32H2O$
Monosulfate	M_1	$C_4A\bar{S}H_{12}$	$(CaO)_4(Al2O3)(SO3) \cdot 12H2O$
Available Sulfates	$\tilde{S}$	$\bar{S} + C\bar{S}$	$SO_4^{2-} + Ca\ SO_4$
Iron	F	F	Fe_2O_3

Aluminium	A	A	Al_2O_3
Available Aluminates	$\tilde{A}$	$A + C_3AH_6$	$(Al(OH)_4^-)_{1/2} + (CaO)_3(Al_2O_3)(H_2O)_6$
Hydrogarnet	G	$C_3AS_yH_{4(3-y)}$	$Ca_3(Al_xFe_{1-x})_2(SiO_4)_y(OH)_{4(3-y)}$
Calcium Silicate Hydrates	CSH	C-S-H	$(CaO)_{1.65}(SiO_2)(H_2O)_{2.45}$
Mass Balance Variables			
Total aluminate	A_c	Total A	Al_2O_3
Total sulfate	S_c	Total $\bar{S}$	SO_3
Equivalent number of moles of alkali	Na_{eq}	Na_{eq}	$Na^+ + K^+$ (3)
Alkali concentration in saturated porosity	(Na)	$\frac{Na_{eq}}{\phi . S_r + k^{(2)} . CSH}$	$[Na^+] + [K^+]$
Ferrite fraction	ρ_F	$\rho_F = \frac{F}{A+F}$	-

(1) if the calculus is performed with the mass instead of the moles number

(2) The coefficient k (0.077 l/mol) concerns alkali fixation in C-S-H. It is calculated according to [24],but this coefficient can also be taken equal to 0 if the heating takes place at early age.

(3) In moles number

Table 2 : Physical Data

Data	Notation	Definition
Temperature	T	Absolute temperature
Concrete porosity	$\emptyset$	Void volume per volume unit of concrete
Free water volume	W	Volume of free water per unit volume of concrete
Saturation rate	S_r	$W/\emptyset$

The total number of moles of sulfates in a unit volume of concrete is noted S_c and the total number of moles of aluminates, A_C. According to [1], due to the solid–liquid equilibrium, the ionic concentrations of aluminates and sulfates are about 100 times smaller than the concentration of calcium or alkali. Therefore these two species are rapidly bound by the production of new phases and their mass transfer can be neglected at the scale of the structure. The mass balances imply that equations (1) and (2) are constantly verified.

$$A_C = E_1 + E_2 + M_1 + G + \tilde{A} \quad (1)$$

$$S_c = 3(E_1 + E_2) + M_1 + \tilde{S} \quad (2)$$

with G, the hydrogarnet (Table 1) that can be formed at high temperature [16].

Alkalis do not act directly in the two reactions but they strongly interfere with other ionic species in thermodynamic equilibrium (fixation of S in C-S-H [18], affect portlandite equilibrium and thus calcium concentration [36]). Only the alkalis are assumed to be significantly mobile at structure scale. They can be fixed reversibly by C-S-H, be leached out of concrete or be consumed in alkali-silica reaction. Their initial concentration in the concrete pore solution thus depends on the saturation degree (Sr) (defined in Table 2) and the amount of C-S-H per unit volume of concrete (Table 1).

The main chemical phenomena considered in this model are:

- Progressive dissolution or delayed formation of Primary Aluminous hydrates (E_1 and M_1) when the temperature exceeds a threshold of dissolution noted $T_{th,d}$. The ionic species, products of the dissolution, are stored in different forms of aluminate (carboaluminates in the case of lime aggregates or lime additions [42]), or hydrogarnet if the temperature is greater than another threshold $T_{th,f}$ [16,36], or can be reversibly bound in the cement matrix. The aluminate available for DEF is noted $\tilde{A}$. The sulfates that are reversibly absorbed in the cement matrix and are available for DEF are noted $\tilde{S}$. $\tilde{A}$ and $\tilde{S}$ are the main state variables of the model.
- Conversion of a proportion of available aluminates $\tilde{A}$ into hydrogarnet (G) if the temperature stays above the threshold value of fixation $T_{th,f}$, for long enough [16].
- Conversion of available aluminates $\tilde{A}$ or M_1 and available sulfates $\tilde{S}$ into secondary ettringite (E_2) when the temperature drops below the threshold of dissolution $T_{th,d}$. If some residual monosulfate M_1 subsists after the heating period, it can be combined with available sulfates $\tilde{S}$ and converted into secondary ettringite [45]. When M_1 is used up, the formation of delayed ettringite also consumes $\tilde{A}$.

Three main impacts on the chemical phenomena have to be quantified in modelling:

- Alkali concentration (Na) acts on the temperature threshold of dissolution $T_{th,d}$ and on the kinetics of dissolution and precipitation of hydrates [5,26,34].
- Temperature (T) activates the diffusion into the unit volume of concrete and activates chemical reactions [27].
- The Water Saturation ratio of the concrete porosity (Sr) can limit the kinetics of DEF precipitation when the temperature is lower than $T_{th,d}$ [43], but it does not limit the dissolution of primary sulfoaluminates at high temperature because water released by ettringite is assumed to allow ions to migrate toward the adsorption sites (specifically C-S-H).

Two other parameters of influence are listed below but are not yet considered in the model because of the lack of experimental results:

- Ferrite fraction, ρ_F(Table 1) which could delay the DEF and modify the kinetics towards the end of the reaction [33].
- Sulfate sorption capability in C-S-H, which could limit the amount of sulfate available for DEF due to a supersaturation in sulfate during the heating period [17].

These last two parameters could have an important impact in cases of blended cement [33]. In fact, in such cements, the ferrite fraction, ρ_F , can be greater than in classic clinker, and the additions can decrease the calcium / silica ratio in C-S-H, which modifies the sulfate sorption capability of the C-S-H. For the sake of simplicity, this limitation is not considered in the present model, where all the sulfates can be absorbed in C-S-H if the heating period is long enough. Concerning the action of the ferrite fraction, it is not explicitly considered but is assumed to be included in the parameters controlling the kinetics of the DEF.

In the present work, the model is specified in the form of differential equations so as to be able to follow the variable evolutions of environmental conditions (temperature, T, water saturation rate, S_r, and alkali concentration (Na)). A differential equation can easily be implemented in any finite element code to compute the amount of DEF, with a time finite difference method for instance. If the environmental conditions are piecewise constant, an analytical solution of the model can be found and used. The analytical solution is especially convenient for fitting the model with spreadsheet software.

Once the chemical model is solved, the amount of DEF is known and can be used in a poro-mechanical model able to compute the structural effects of expansion [23] [22]. This mechanical aspect of the modelling can be decoupled from the chemical ones since the pressure induced by the DEF remains lower than the thermodynamic pressure needed to stop the chemical reaction. According to [11] cited in [2], the crystallization pressure is proportional to the logarithm of the activity product. The activity product can be very high in the concrete porosity since the available species involved in the DEF are supplied by an amount of cement that is large relative to the volume of free water. As concrete can crack at low pressure due to its low tensile strength, the mechanical pressure is considered never to be sufficient to limit the DEF in this simplified model. In addition, due to the concrete pore microstructure, not all the DEF participates in expansion [19]. This is also considered in the proposed poro-mechanical model [22,23].

2 Chemical Model Formulation

2.1 State variables and initial conditions for the chemical problem

For any simulation of DEF, the process begins with the determination of the initial conditions for the different state variables of the model. The state variables are the ones corresponding to the set called "Hydrates and Ions (free or absorbed)" in Table 1. Their determination results from the compatibility between anhydrous phases and hydrates. To simplify the model, ferrites and aluminates are first merged in an equivalent moles number of C_3A noted C_3A^{eq}:

$$C_3A^{eq} = C_3A + 2C_4AF = A + F \quad (3)$$

Then the total number of moles of aluminates A_c and sulfate S_c provided by the cement are computed:

$$A_c = C_3A^{eq} \quad (4)$$

$$S_c = \bar{S} \quad (5)$$

with $\bar{S}$ the sulfate contained in the initial gypsum (Table 1).

According to the molar ratio of sulfate / aluminate, the different state variables are initialized as follows. These relations can be easily retrieved using the stoichiometry of the hydration reactions. If the ratio is greater than 3, primary ettringite can be created:

$$\text{If } \left(\frac{S_c}{A_c}\right) > 3 \Longrightarrow \begin{cases} E_1 = A_c \\ M_1 = 0 \\ \tilde{A} = 0 \\ \tilde{S} = S_c - E_1 \\ G = 0 \\ E_2 = 0 \end{cases} \quad (6)$$

If the sulfate / aluminate ratio is between 1 and 3, mono- and tri-sulfoaluminates coexist:

$$\text{If } 1 \leq \left(\frac{S_c}{A_c}\right) \leq 3 \Longrightarrow \begin{cases} E_1 = \frac{S_c - A_c}{2} \\ M_1 = \frac{3A_c - S_c}{2} \\ \tilde{A} = 0 \\ \tilde{S} = 0 \\ G = 0 \\ E_2 = 0 \end{cases} \quad (7)$$

If the sulfate/aluminate ratio is lower than 1, only monosulfate exists and residual aluminates are stored in variable $\tilde{A}$:

$$\text{If } \left(\frac{S_c}{A_c}\right) < 1 \Longrightarrow \begin{cases} E_1 = 0 \\ M_1 = S_c \\ \tilde{A} = A_c - M_1 \\ \tilde{S} = 0 \\ G = 0 \\ E_2 = 0 \end{cases} \quad (8)$$

2.2 Mass balance equations

Two cases have to be envisioned:

- The temperature is greater than or equal to the dissolution threshold, $T_{th,d}$. This leads to dissolution of the primary hydrates (E_1, M_1) (or avoids their formation if the heating cycle takes place at early age) to produce free forms of aluminates ($\tilde{A}$) available to form carboaluminates in presence of lime, or hydrogarnet if the temperature is kept higher than the fixation threshold, $T_{th,f}$, for long enough.
- If the temperature is lower than the dissolution threshold, $T_{th,d}$, the free aluminates ($\tilde{A}$), sulfates ($\tilde{S}$) and the monosulfate (M_1) can be combined to produce DEF.

2.2.1 Chemical reactions at temperatures higher than the dissolution threshold $T_{th,d}$

When the temperature allows the dissolution of sulfoaluminates, ettringites - whether they are in a primary or a secondary form (E_1 and E_2) - and the monosulfate M_1 are destabilized [13–15], (equation set 9):

$$\begin{cases} \frac{\partial E_1}{\partial t} = -\frac{E_1}{\tau_d} \\ \frac{\partial M_1}{\partial t} = -\frac{M_1}{\tau_d} \\ \frac{\partial E_2}{\partial t} = -\frac{E_2}{\tau_d} \end{cases} \quad (9)$$

with τ_d the characteristic time for the dissolution processes. The dissolution of the three species is not instantaneous. The characteristic time translates the progressivity of the dissolution processes associated with the diffusion and sorption of released ions. A single characteristic time is used for sake of simplicity. As illustrated below, the results obtained with this simplification are in good accordance with experimental results. Even if the different sulfo-aluminates hydrates have different sensitivity towards the temperature rising, the diffusion of dissolved species and their fixation are certainly slower than the thermodynamic destabilization. Thus, it is not necessary to use different characteristic times for the different sulfo-aluminate hydrates. The species released by the dissolution lead to an increase of free aluminates ($\tilde{A}$) and sulfates ($\tilde{S}$). The sulfates are assumed to be reversibly bound in cement hydrates [17]. They remain available for the DEF:

$$\frac{\partial \tilde{S}}{\partial t} = -3\left(\frac{\partial E_1}{\partial t} + \frac{\partial E_2}{\partial t}\right) - \left(\frac{\partial M_1}{\partial t}\right) \quad (10)$$

At high temperature ($T > T_{th,f}$) the free aluminates ($\tilde{A}$) can be converted to hydrogarnet (G) [16,36], or carboaluminates in presence of limes. The kinetics of the production of hydrogarnet and carboaluminates depends on the amount of aluminate released from primary hydrates: the greater the amount of aluminate released, the greater the production of hydrogarnet or carboaluminate. The dependence is given by equation (11):

$$\frac{\partial \mathrm{G}}{\partial t} = \frac{\tilde{A}}{\tau_f} \quad (11)$$

with τ_f the characteristic time for the fixation of aluminates in hydrogarnets or carboaluminates. Due to this reaction, the mass balance equation of free aluminates ($\tilde{A}$) has to consider this possibility:

$$\frac{\partial \tilde{A}}{\partial t} = -\left(\frac{\partial E_1}{\partial t} + \frac{\partial E_2}{\partial t} + \frac{\partial M_1}{\partial t}\right) - \frac{\tilde{A}}{\tau_f} \quad (12)$$

Using the mass balance equations (1) and (2) in (12) leads to the following differential equations:

$$\begin{cases} \frac{\partial \tilde{A}}{\partial t} = \frac{A_c - G - \tilde{A}}{\tau_d} - \frac{\tilde{A}}{\tau_f} \\ \frac{\partial \mathrm{G}}{\partial t} = \frac{\tilde{A}}{\tau_f} \end{cases} \quad (13)$$

If the characteristic times τ_d and τ_f remain constant during a period $\Delta t = t - t_0$, and the threshold temperatures both exceeded, the two differential equations (13) can be merged into one:

$$\frac{\partial^2 \tilde{A}}{\partial t^2} + \left(\frac{1}{\tau_d} + \frac{1}{\tau_f}\right)\frac{\partial \tilde{A}}{\partial t} + \frac{\tilde{A}}{\tau_d \tau_f} = 0 \quad (14)$$

This last equation admits an analytical solution given in the appendix. This solution can be used to fit the model from an experimental result obtained with a thermal cycle presenting a substantial temperature plateau or, in a finite element context, to improve the numerical accuracy for a time step Δt, during which the environmental conditions can be considered as fixed.

2.2.2 Chemical reaction at temperature lower than the dissolution threshold $T_{th,d}$

The aluminates $\tilde{A}$ and sulfates $\tilde{S}$ available for DEF depend on the duration of the heating period. They are computed during the hot period using the equation set presented above. When the heating period ends, concrete returns to the ambient temperature $T < T_{th,d}$. The dissolution of sulfoaluminates and the formation of hydrogarnet are then no longer possible, but DEF can occur. The DEF is also modelled by a differential equation able to consider variations of environmental conditions. As shown in [36], the DEF kinetics is mainly controlled by the release of sulfates bound in

the cement matrix, so in the present simplified modelling this phenomenon is assumed to control totally the precipitation kinetic:

$$\frac{\partial E_2}{\partial t} = \frac{\tilde{S}}{\tau_p} \tag{16}$$

τ_p is the characteristic time to control the precipitation kinetics. It depends on the water saturation rate S_r, which allows the different chemical species to move towards one another by diffusion under the influence of the chemical affinity of the reaction. It also depends on the alkali concentration (Na), which favours the retention of sulfates in C-S-H, delaying their release into the pore solution according to the model of Salgues et al [36], and possibly on the ferrite fraction, ρ_F, because ettringite containing Fe is generally created more slowly than that with Al [33].

If monosulfates M_1 subsist after the hot period, sulfates can be combined with them to form delayed ettringite [45]. As M_1 already contains one mole of aluminate and one mole of sulfates, the evolution of the state variables is then:

$$\begin{cases} \frac{\partial M_1}{\partial t} = -\frac{\partial E_2}{\partial t} \\ \frac{\partial \tilde{S}}{\partial t} = -2\frac{\partial E_2}{\partial t} \\ \frac{\partial \tilde{A}}{\partial t} = 0 \end{cases} \tag{17}$$

Once all the monosulfates M_1 have been consumed by reactions (17), if some $\tilde{S}$ subsist, the DEF continues to consume $\tilde{A}$ as follows:

$$\begin{cases} \frac{\partial M_1}{\partial t} = 0 \\ \frac{\partial \tilde{S}}{\partial t} = -3\frac{\partial E_2}{\partial t} \\ \frac{\partial \tilde{A}}{\partial t} = -\frac{\partial E_2}{\partial t} \end{cases} \tag{18}$$

The delayed ettringite formation stops when no more sulfates or aluminates remain.

2.3 Assessment of the destabilization threshold temperature $T_{th,d}$

The destabilization of ettringite at high temperature can be ideally modelled in a thermodynamic context using a Van't Hoff equation, which gives the evolution of the solubility constant [13] versus temperature as in the model presented in [36]. Such thermodynamic modelling needs to solve the mass balance equations simultaneously for all chemical species involved in the equilibrium equations. The resulting numerical problem becomes too computer-time consuming to be used in a finite element context also involving numerous other nonlinear problems (creep, plasticity, damage, poro-mechanics, and reinforcements). So, a simplification is proposed, which can be used in a

context of coupling with non-linear mechanical problems in order to consider the dependence of the threshold temperature on the chemical context. Kchakech [26] proposed an empirical law deduced from Brunetaud's experimental results [5] and based on the dependence on the alkali concentration. This law is adapted here to have a normalisation parameter, Na_k in equation (19). It allows having a relationship form independent of the unit system used. More, the parameter is also used as threshold value, in order to avoid obtaining too high temperature for low alkali concentration:

$$T_{th,d} = T_0 + \begin{cases} T_{th,ref} & Na < Na_k \\ T_{th,ref}\left(\frac{Na_k}{Na}\right)^n & Na \geq Na_k \end{cases} \quad (19)$$

The fitting of equation (19) on results supplied by Brunetaud [5] corresponds to $T_{th,ref} = 80^\circ C$ for $Na_k = 0.28\, mol/l$ and $n = 0.19$. It is illustrated in Figure 1. In equation (19), the threshold temperature can be changed from degrees Celsius to Kelvin for further applications with $T_0 = 273.15\, K$.

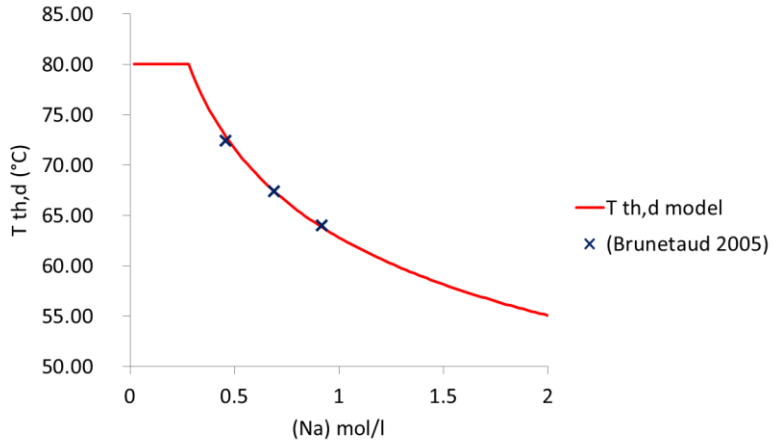

Figure 1 : Temperature threshold evolution, model fitted on Brunetaud's results

In Figure 1, experimental results come from Brunetaud's experimental observations [4,5]. As these results come from a single author, the law proposed by Kchakech [26] could be affected by the cement composition and should be verified experimentally for alkali contents outside this fitting range.

2.4 Influence of environmental conditions on reaction kinetics

The characteristic times (τ_d, τ_f, τ_p) used in the mass balance equations (9, 11, 16) to control the reaction kinetics depend on environmental conditions: temperature (T), moisture (H) and chemical conditions (C). Although the lack of data remains the main problem in clarifying this part of the model, evolution laws are needed so that the different environmental conditions of real structures

can be considered. Their fitting is addressed in the section dedicated to the model application. To consider the THC (Thermo-Hydro-Chemical) effects systematically, each characteristic time of the model is modified by three coefficients as follows:

- The characteristic time τ_d used in the equation of dissolution of primary sulfoaluminates (9) is modified by coefficients C_d^T, C_d^H, C_d^C:

$$\frac{1}{\tau_d} = \frac{1}{\tau_d^{ref}} C_d^T C_d^H C_d^C \quad (20)$$

- The characteristic time τ_f controlling the uptake of aluminate (equation 11) is modified as follows:

$$\frac{1}{\tau_f} = \frac{1}{\tau_f^{ref}} C_f^T C_f^H C_f^C \quad (21)$$

- The characteristic time τ_p controlling the precipitation of secondary ettringite at low temperature (equation 16) is modified in a similar way:

$$\frac{1}{\tau_p} = \frac{1}{\tau_p^{ref}} C_p^T C_p^H C_p^C \quad (22)$$

These nine coefficients C require a very large experimental plan if they are to be fitted accurately. Nevertheless, the theoretical knowledge of some phenomena highlighted by thermodynamic considerations such as Arrhenius thermal activation of diffusion for C_d^T [27], chemical equilibrium conditions for C_d^C [14,15]. Experimental observations can also be used, such as absence of swelling below a given saturation rate for C_p^H [44] or above a given alkali concentration [5] for C_p^C. All these information can guide the choice of reasonable laws which can then be fitted from the experimental results available in the literature. Note that the characteristic times above also depend on other physical phenomena like concrete porosity or thermal damage, but these influences are considered as factors that affect the concrete permanently, so they are somehow already included in the reference values of characteristic times.

2.4.1 Influence of the temperature on the kinetics

Temperature impacts chemical reactions by the activation of micro diffusion processes. This effect can be considered with an Arrhenius law [27]. A loss of chemical affinity of DEF also has to be considered when the temperature is close to the dissolution threshold $T_{th,d}$. It could be modelled by the Van't Hoff law if all the ionic species involved in the DEF were considered in the model [13], as is the case in [36] for instance. In the present model, for the sake of simplicity, only sulfates, aluminates and alkali are considered. It is then no longer possible to use the Van't Hoff law directly. The thermal

effects are simplified by combining the Arrhenius and Van't Hoff laws in a single approximation. The best fit concerning the dissolution and fixation processes (when $T > T_{th,d}$) were obtained with the following laws:

$$C_d^T = exp\left(-\frac{\mathrm{Ea}_d}{R}\left(\frac{1}{T}-\frac{1}{T_{th,d}}\right)\right) - 1 \quad \geq 0 \tag{23}$$

$$C_f^T = exp\left(-\frac{\mathrm{Ea}_f}{R}\left(\frac{1}{T}-\frac{1}{T_{th,f}}\right)\right) - 1 \quad \geq 0 \tag{24}$$

with Ea_d and Ea_f the activation energy of dissolution and fixation mechanisms respectively.

Experiments modelled in the sections below show that $T_{th,f}$ is independent of the alkali content, and a value close to 70°C seems acceptable to explain the absence of a pessimum effect of heating duration for specimens heated to 65°C, while, according to Kchakech [26] specimens heated to 71°C present a very low pessimum effect, and that this pessimum effect is more pronounced at higher temperature.

When the temperature is lower than the dissolution threshold ($T < T_{th,d}$), only the DEF is active. The dependence of the DEF kinetics on the temperature is then driven by the Arrhenius law on precipitation mechanisms.

$$C_p^T = exp\left(-\frac{\mathrm{Ea}_p}{R}\left(\frac{1}{T}-\frac{1}{T_p^{ref}}\right)\right)\frac{C_d^T(T)}{C_d^T\left(T_p^{ref}\right)} \tag{25}$$

with Ea_p the activation energy of precipitation. To facilitate the calibration of this parameter, the reference temperature T_p^{ref} can be chosen independently of $T_{th,d}$, which is why the normalization term $C_d^T\left(T_p^{ref}\right)$ appears in equation (25). As the literature supplies contradictory tests results for specimens stored at different temperatures during the DEF, the calibration of activation energy Ea_p is not yet feasible: in [19], the specimen does not swell at 38°C, while in[29], this same temperature allows to accelerate swelling. Therefore, a value close to the one usually used in hydration models ($Ea_p \approx 44\mathrm{kJ/Mol}$) is adopted to illustrate the method chosen to consider effect of temperature on DEF kinetics [6]. It will have to be readjusted as soon as adequate experimental results will be available.

The evolutions of thermal coefficients are illustrated in Figure 2 for a dissolution threshold chosen equal to $T_{th,d} = 65°C$. This value is chosen arbitrarily among the different values possible in Figure 1. It could be obtained for instance using a high alkali concentration during heating of about 0.8 mol/l

according to equation 19 fitted on Brunetaud's experimental results [5], in low alkali cement this temperature is greater as illustrated in Figure 1. The three kinetics: dissolution of primary sulfoaluminates (C_d^T in Figure 2), fixation of aluminates (C_d^T), and precipitation of secondary sulfoaluminates (C_p^T) are null at the point corresponding to this threshold temperature. For the modelling presented in this figure, precipitation of sulfoaluminates stops for temperatures higher than 65°C and dissolution begins above this temperature (Figure 2), while the aluminate fixation starts for temperatures higher than 70°C.

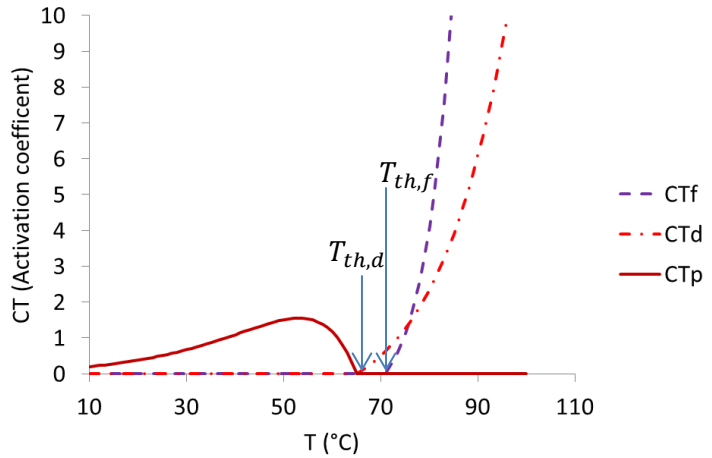

Figure 2 : Thermal activation coefficients versus temperature for dissolution of primary sulfoaluminate hydrates (CTd), fixation of aluminate in hydrogarnet at high temperature (CTf) or precipitation of secondary ettringite (CTp) (example for a threshold dissolution temperature of 65°C corresponding to a high alkali content (0.8 mo/l), and a threshold fixation temperature of 70°C Eap=44 kJ/mol, Ead 80 kJ/mol and Eaf=180 kJ/mol)

2.4.2 Influence of alkali on kinetics

At given temperature and humidity, a high alkali concentration promotes the sorption of sulfates in the cement matrix [18,34] and consequently accelerates the dissolution of primary sulfoaluminates. This effect is considered in the model by reducing the characteristic time of dissolution τ_d with the coefficient C_d^C:

$$C_d^C = \left(\frac{Na}{Na_k}\right) \tag{26}$$

with $Na_k = 0.28\, mol/l$, the alkali concentration in the saturated porosity already used as normalization parameter in equation (19).

The analysis of Kchakech's results [26] by this model shows that the kinetics of aluminate fixation (considered with C_f^C in equation 21) has to be modified according to the alkali content. It has to

evolve inversely to the alkali concentration and faster than C_d^C, which is why the fitting parameter m in equation (27) must be set equal to 3 to adjust the model to experimental results:

$$C_f^C = \left(\frac{Na_k}{Na}\right)^m \quad (27)$$

The evolutions of these coefficients are illustrated in Figure 3. The modification of the kinetics of these two phenomena with alkali content was already observed by Martin and Kchakech [26] and considered in their phenomenological models. Only the shape of the laws have been modified to obtain a calibration of the present model with all the experiments considered just below. Finally, Figure 3 sums up the effects of alkali on the kinetics involved in sulfoaluminate dissolution. The larger the initial alkali concentration:

- the faster the sulfoaluminate dissolution; it can be modelled by a linear relationship,
- the slower the aluminate fixation, with a nonlinear equation.

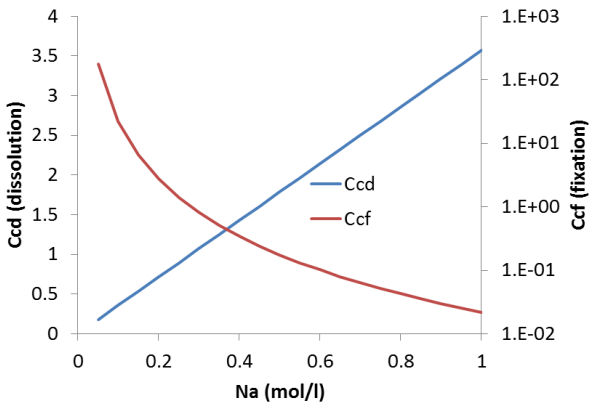

Figure 3: Effect of alkali concentration on dissolution and fixation kinetics during heating period (Nak=0.28 mol/l, m=3)

Due to their influence on the sorption of sulfates, alkalis have an effect during DEF at low temperature that is the inverse of that during dissolution at high temperature. As illustrated in the application section below, a high concentration reduces the kinetics of DEF [18]. This is modelled by equation (28):

$$C_p^C = \begin{cases} \left(1 - \frac{Na}{Na^{bl}}\right)^m, & if\ Na < Na^{bl} \\ 0, & if\ \ Na \geq Na^{bl} \end{cases} \quad (28)$$

The evolution of the kinetic coefficient is illustrated in Figure 4 with $Na^{bl} = 0.92\ mol/l$ and $m = 3$ (fitted on Famy's results illustrated in Figure 9): the larger the alkali concentration, the slower the DEF. The value of Na^{bl} depends on the concrete mix, a Na^{bl} twofold the initial alkali concentration matches well enough with experimental results considered in this work. The curve in Figure 4

explains why DEF tests are faster in storage conditions allowing alkali leaching (since the DEF kinetic increases with the low alkali concentrations).

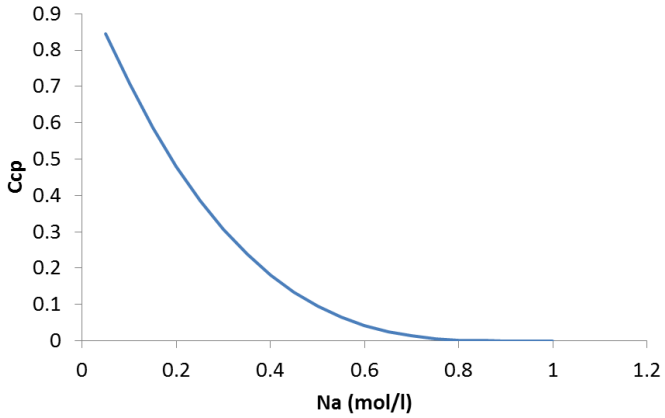

Figure 4 : Evolution of C_p^C versus alkali concentration (Na_{bl}=0.92mol/l, m=3)

2.4.3 Influence of water saturation on kinetics

Sulfoaluminates are assumed to be able to dissolve whatever the saturation rate. However, they need water to precipitate because ions have to move by diffusion in the pore solution to create local stoichiometric conditions of ettringite precipitation; moreover water is a reactant. For the sake of simplicity, the dissolution and fixation phenomena are possible whatever the saturation (C_d^H and C_f^H are set equal to one). Only C_p^H, used in equation (23), which controls the precipitation rate, presents any great dependence on the saturation. According to [43], the DEF kinetics is measurable in laboratory conditions and with an acceptable experiment duration (about 3 years) only close to the saturation condition, leading to relationship (29) for C_p^H. As soon as the porosity is no longer saturated, the diffusion of ions rapidly becomes difficult and the kinetics of precipitation decreases drastically. This leads to a highly nonlinear equation:

$$C_p^H = exp\left(-\frac{1-S_r}{1-S_r^k}\right) \quad (29)$$

The evolution of C_p^H is illustrated in Figure 5 for three different values of the fitting parameter S_r^k.

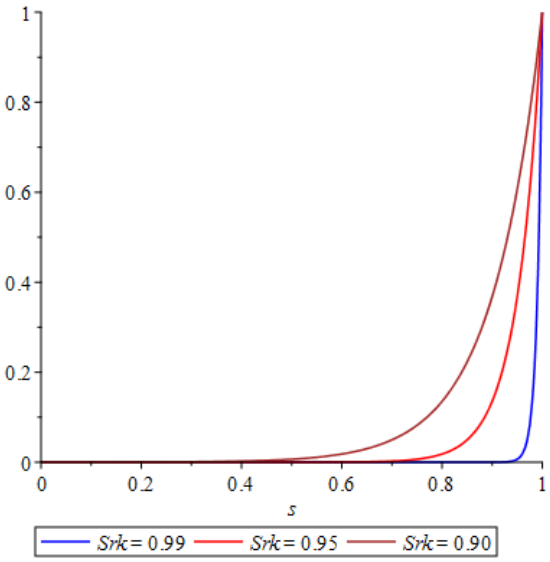

Figure 5 : Effect of water saturation on precipitation kinetics of sulfoaluminates

If the saturation degree is equal to S_rk, the kinetics of precipitation is reduced by 60% compared to its value in the saturated condition (Figure 5). A value of S_rk greater than or equal to 95% is needed to explain the observations of [43]. In his PhD thesis, Al Shamaa shows that specimens stored at 98% RH have a water mass intake four times slower than at 100% RH. This phenomenon can be explained by a DEF kinetics four times slower at 98% than at 100%, corresponding approximately to a S_rk of 95%. It is obvious that this great nonlinearity of the DEF kinetics versus the saturation ratio S_r could be problematic for the prediction of DEF in non-saturated structures, for which the determination of S_r remains a challenge in itself.

2.5 Calibration and application of the chemical model

2.5.1 Materials

In this section, five materials are studied with the chemical model presented above These materials (Table 3) were chosen because their compositions, heating conditions and conservation conditions are well-described in the corresponding publications [4,18,26,29]. For all these materials, expansions were measured until stabilization. Different heating conditions were used, and the chemical model parameters could be calibrated by considering the dissolution and fixation phenomena [5,26]. With these five materials, the cement composition or alkali content present large enough variations to fit the alkali effects considered in the model. The conservation conditions were also evaluated in terms of alkali leaching possibility through literature data [18], in order to fit the effect of the alkali concentration in the pore solution on DEF kinetics. Among these materials, four are concrete and one is a mortar (the material studied by Famy).

In these applications the alkali concentration in the pore solution was computed assuming that part of the alkali (Na^B) was bound in the C-S-H:

$$Na^B = k.CSH.(Na) \quad (30)$$

Using the mass balance of alkali (31) then leads to a conventional alkali concentration in pore water (32):

$$\phi.Sr.(Na) + k.CSH.(Na) = 2\,Na_2O_{eq} \quad (31)$$

In (31), according to [36], $k \sim 0.077\ l/mol$. The moles number of C-S-H for clinker can be assessed using the moles number of silicate divided by its stoichiometric coefficient in C-S-H (1.65 for plain clinker cements), and multiplied by the hydration rate [7].

$$(Na) = \frac{2\,Na_2O_{eq}}{\phi.Sr + k.CSH} \quad (32)$$

Equation (32) is given for further applications of the model. However, for the following analysis, the alkali concentration was either given by the authors (these materials are the ones, with superscript (1) in Table 3), or for the others, it was imposed through an alkali supply during the concrete mix. More, for some of them, the heating cycles are applied at very early age. In this case, the alkali are not yet bounded in C-S-H during the primary ettringite destabilisation at high temperature, so the alkali concentrations can be assessed, neglecting the term k.CSH comparatively to φ.Sr, (superscript (2) in Table 3). Concerning the saturation rate Sr, as all specimens were stored in water, it is taken equal to one. In Table 3, the oxides are given in % of cement mass.

Table 3: Materials used to calibrate the model from [4,18,26,29]

Author/ Material	Cement (kg/m3)	Ø (%)	CSH (mol/m^3)	Al_2O_3 (%)	Fe_2O_3 (%)	SO_3 (%)	Ac Mol/m3	Sc Mol/m3	Sc/Ac -	(Na) Mole/l
Brunetaud[3]	400	14	884	4.1	3.75	3.36	255	168	0.66	0.92[1] 0.69[1] 0.46[1]
Kchakech R0[3]	410	15.2	1078	3.33	3.83	2.61	232	134	0.58	0.38[1]
Kchakech R1[3]	410	15.2	974	4.3	3.8	3.46	270	177	0.66	0.84[1]
Famy[2]	500	25	1274	5.4	2.2	3.9	333	244	0.73	0.53[1]
Martin[3]	410	14.6	974	4.3	3.8	3.46	270	177	0.66	0.91[1]

(1) Alkali computed from initial conditions, neglecting the fixation in C-S-H at early age, and assuming a water saturation of the porosity

(2) Mortar

(3) Concrete

The parameters necessary to determine the dissolution of primary sulfoaluminates and the fixation of aluminate at high temperature (listed in Table 5) are fitted on the final expansion (asymptotic values of swelling) measured for the concrete studied in these five experiments given in Table 4. For the sake of simplicity, and to avoid resorting to the mechanical part of the model presented in the next section, the final expansion is assumed to be proportional to the delayed ettringite amount, which depends on the conditions during the heating period (duration and temperature of the heating, alkali concentration during this period). The volume change of the specimen is taken to be isotropic as observed in [3] and DEF volume is assumed to be totally reported in the swelling to a first approximation. The volume change is thus assumed to be 3 times the measured axial expansion. So, during this simplified calibration, the DEF volume obtained by the chemical modelling is divided by 3 compared to the free uniaxial swelling measured during the experiment. Thus a DEF volume of 6% is assumed to correspond to an isotropic volumetric swelling of 6%, which is equivalent to a specimen change of length of 2% in each direction. This assumption is only made for the calibration of the parameters of the chemical model as the combination with mechanical considerations would lead to complex calibration for all these five experiments. In real structure conditions, the poro-mechanical modelling takes account of the interaction with concrete microstructure and mechanical properties, and computed expansions will not always be proportional to the ettringite amount as explained below.

Table 4 : Environmental conditions and final swellings

Author, heating temperature, heating duration (plateau only)	Experimental final expansion (specimen relative length change %)		
Alkali concentration (Na) for Brunetaud's tests	*0.92 mol/l*	*0.69 mol/l*	*0.46 mol/m*
Brunetaud 85°C 2h	0.40	0.40	0.014
Brunetaud 85°C 6h	0.40	0.40	0.014
Brunetaud 85°C 48h	1.20	1.20	0.91
Brunetaud 85°C 240h	0.02	0.20	0.09
Brunetaud 65°C 2h	0.01		
Brunetaud 65°C 6h	0.01		
Brunetaud 65°C 48h	0.05		
Brunetaud 65°C 240h	0.5		

Kchakech R0 81°C 25h	0.03
Kchakech R0 81°C 73h	0.44
Kchakech R0 81°C 169h	0.40
Kchakech R0 81°C 337h	0.04
Kchakech R1 81°C 25h	1.25
Kchakech R1 81°C 73h	1.74
Kchakech R1 81°C 121h	1.66
Kchakech R1 81°C 169h	1.45
Kchakech R1 81°C 337h	0.89
Kchakech R1 71°C 54h	0.49
Kchakech R1 71°C 175h	1.33
Kchakech R1 71°C 288h	1.51
Kchakech R1 71°C 341h	1.48
Kchakech R1 71°C 677h	1.22
Kchakech R1 66°C 345h	0.25
Kchakech R1 61°C 347h	0.00
Famy 90°C 12h	1.00
Martin 80°C 72h	1.60

2.5.2 Global fitting of DEF potential

For each material and each heating condition, the analytic solutions of equations (9, 10, 14) giving aluminates $\tilde{A}$, sulfates $\tilde{S}$ and residual mono-sulfoaluminates M_1 are used to compute the number of moles of reactive species able to produce ettringite in the long term. Then the maximal amounts of ettringite in the long term in saturated and alkaline leaching conditions are computed (asymptotic values of equation (17) and (18)) and used to assess the volume of delayed ettringite (by multiplying the number of moles by the molar volume of ettringite: 715 cm^3/mol according to [1,20]). Figure 6 shows the correlation between the third of calculated DEF volume and the experimental final swelling. All the points in Figure 6 were obtained with the single parameter set given in Table 5. Once fitted, the model is able to explain more than twenty different experiments performed with different materials, alkali contents and heating durations. The prediction capability corresponding to coefficient R^2 in Figure 6 is close to 90%. The model presents a better prediction capability for large swellings than for smaller ones. Effectively, from a physical point of view, the final swelling cannot be linked to the DEF volume so easily: on the one hand, the chemistry description level proposed in this model contains many simplifications and, on the other hand, mechanical aspects play a non-negligible role in linking DEF volume and swelling [19]. In the poro-mechanical model used below, a

464 certain amount of DEF is first used to fill a part of the porosity connected to the sites of ettringite
465 precipitation without causing pressure, as analysed in [19]. This connected porosity thus absorbs part
466 of the DEF without causing expansion (like the gel of alkali-silica reaction in [35]). For DEF, it could
467 correspond to pores that are too large to lead to damaging pressure. As expansion does not involve
468 the entire DEF amount, this can also explain why the slope of the correlation line (0.9 in Figure 6) is
469 lower than one, and why the swelling is overestimated more often for small swellings than for large
470 ones.

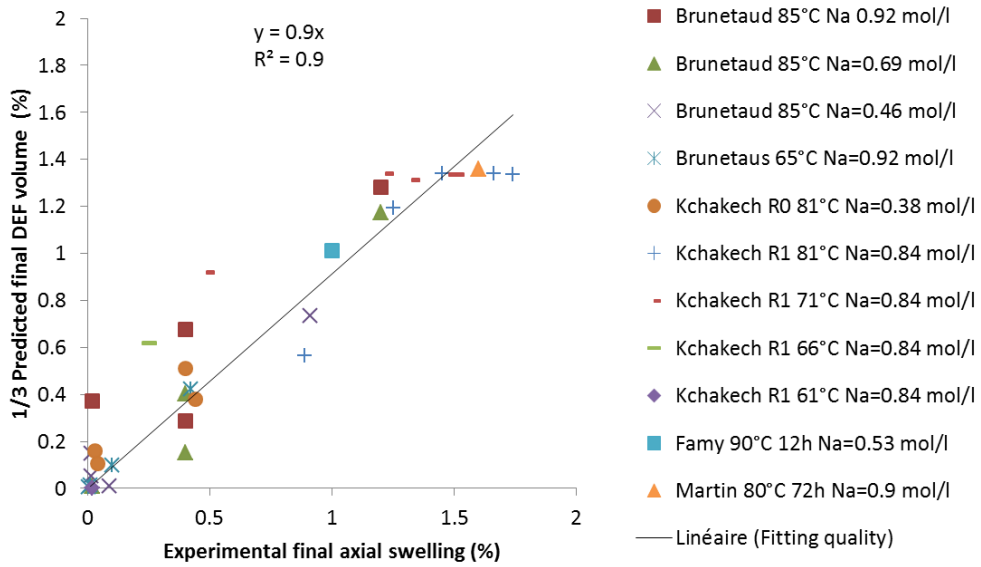

471

472 **Figure 6 : Overview of prediction capability of the model with single parameter set (given in Table 5)**

473 **Table 5: Model parameters corresponding to the global fitting**

Parameter	Equation	Physical meaning	Fitted value	Unit
$T_{th,ref}$	(19)	Dissolution temperature at Na_k	80	°C
Na_k	(19) (27) (28)	Characteristic alkali concentration	0.28	mol/l
n	(19)	Exponent for the dissolution temperature low	0.18	-
$\tau_d^{ref\,(1)}$	(20)	Characteristic time for the dissolution (at high temperature)	65	hour
$\tau_p^{ref\,(1)}$	(22)	Characteristic time for the DEF	30	day
$\tau_f^{ref\,(1)}$	(21)	Characteristic time for the fixation of	30	hour

		aluminates (at high temperature)		
$T_{th,f}$	(24)	Threshold temperature for the fixation of aluminates	70	°C
Ea_d	(23)	Energy activation for the dissolution processes at high temperature	80,000	J/mol
Ea_f	(24)	Energy activation for the fixation of aluminates at high temperature	180,000	J/mol
Ea_p	(26)	Energy activation for the DEF	44,000	J/mol
T_p^{ref}	(26)	Reference temperature used to define τ_p^{ref}	20	°C
m	(27) (28)	Exponent for the lows considering the limiting effect of Na on aluminate fixation and DEF	3	-
Na^{bl}	(28)	Alkali concentration above which the DEF is impeded	0.96	mol/l
S_r^k	(29)	Characteristic saturation rate below which the DEF is limited	0.95	-

(1) Characteristic times correspond to environmental condition for which the temperature, saturation rate and alkali content leads to coefficient C^T,C^H and C^C equal to the unit.

2.5.3 Effect of heating duration (analysis of Brunetaud's results)

To highlight the effects of heating duration and alkali content during heating, Brunetaud's experimental results are summarized in Figure 7, which shows the final swelling of specimens free of stresses versus heating duration. In this figure, the plain lines link the final swelling predicted by the model and the points represent the swelling values at the end of the experiments [5]. For initial heating cycles at 85°C, the final swellings present a maximum for a heating duration close to 50 hours. The amplitude of this swelling depends on the alkali content: the higher the initial alkali content, the larger the swelling. For heating cycles at 65°C, the pessimum effect does not exist for the heating durations analysed in this experimentation. The swelling is smaller than at 85°C and appears to be proportional to the heating duration. In the model, the absence of pessimum at 65°C is explained by the impossibility of creating hydrogarnet to fix aluminates during heating below $T_{th,f}$ = 70°C. At 85°C, this possibility exists and leads to progressive fixation of aluminates with the heating duration, depriving DEF of one of its constituents. Two parametric studies are now given to analyse the influence of model parameters. In Figure 7, the effects of the characteristic times (with +/-10% variation) are given. The impact of the characteristic times on final expansion is small. The maximum

deviation is for high duration with variation of about 20% of the final expansion for the variation of 10% of the characteristic times. In Figure 8, the reference solutions (plain lines) are compared with two others for which the threshold temperature of fixation of Al in Hydrogarnet varies of +/-5°C. Results show clearly the great impact of this last parameter which controls the amplitude of final swelling for specimens with long heating. The higher the threshold temperature of fixation of Al, the higher the final swellings, except for the heating at 65°C which is not sensible to this parameter and presents none pessimum for the duration studied here. In the model, this is the consequence of a heating temperature lower than the minimal temperature required to fix Al in Hydrogarnet.

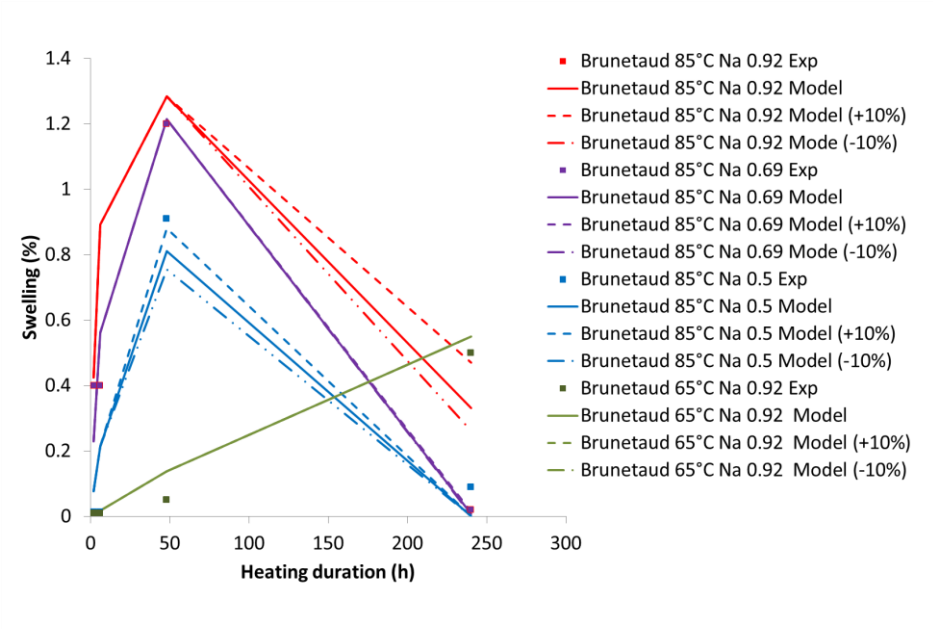

Figure 7 : Prediction of final swelling (lines) versus heating duration for Brunetaud's tests, compared to experimental results (point) (parametric study with +/-10% on characteristic times of dissolution and fixation dotted lines)

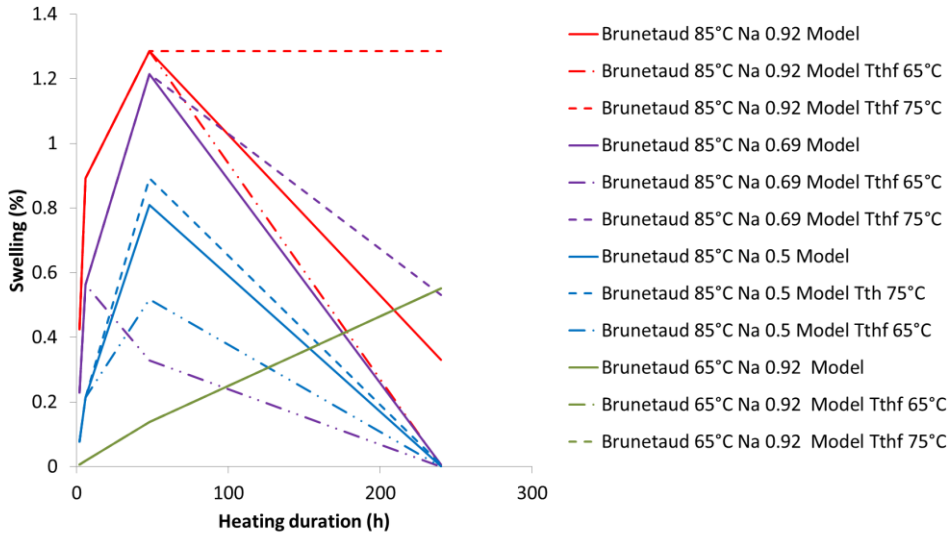

Figure 8 : Prediction of final swelling versus heating duration for Brunetaud's mix : parametric study with +/-5°C on threshold temperature of Al fixation during hot period ($T_{th,f}$)

2.5.4 Effect of alkali concentration during DEF (analysis of Famy's results)

To show the influence of alkali on DEF, Famy carried out a series of experiments in which the specimens were heated in similar conditions but stored in water with different alkali concentrations [18]. As illustrated in Figure 9, the higher the alkali concentration during DEF, the slower the DEF kinetics. In this experiment, a concentration of 0.92 mol/l was able to prevent DEF expansion. In the model, the slowdown of DEF kinetics is obtained by the coefficient C_p^C (equation 28), which depends on alkali concentration as illustrated in Figure 4. The fitted parameter is Na_{bl} (given in Table 5). It is obtained by error minimization using a classical least square method which minimizes the difference between computed and experimental curves. The diffusion is first modelled. Calculus are performed assuming an initial concentration of 0.53 mol/l during the heating period, and the different boundary conditions are in accordance with the storage conditions specified by Famy [18].

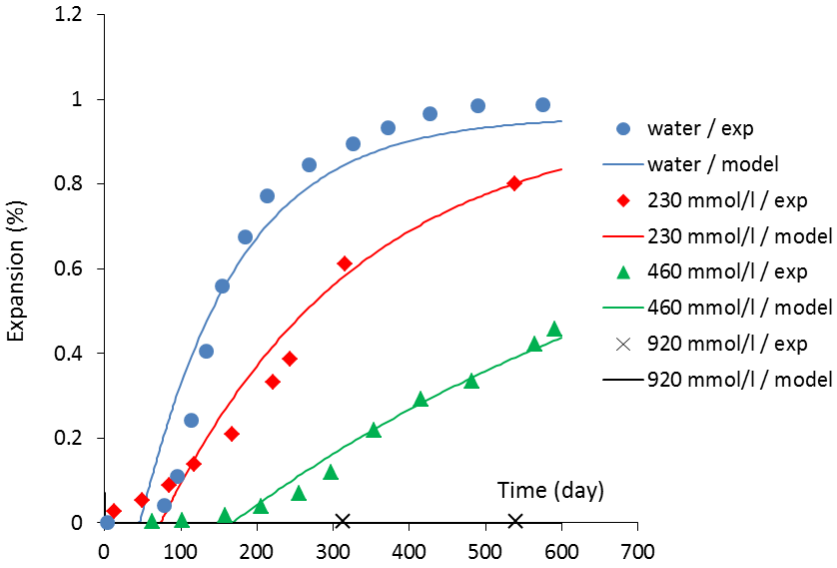

Figure 9: Influence of KOH concentration in the storage bath on kinetics of DEF. Mortar was initially at 530mmol/l of Na^{eq}: comparison between model (lines) and Famy's experimental results (symbols)

3 Chemo-mechanical Model Formulation

3.1 Poro-mechanical formulation

To illustrate the different features of the chemical model and its coupling with a mechanical finite element code, the chemical model presented above was implemented with a nonlinear mechanical model [39] already used in a close form to consider structural effects of alkali aggregate reaction (AAR) [23]. This model is able to consider the effect of pressure (Pg) in a part of the porosity of concrete through equations (33) as illustrated in Figure 10.

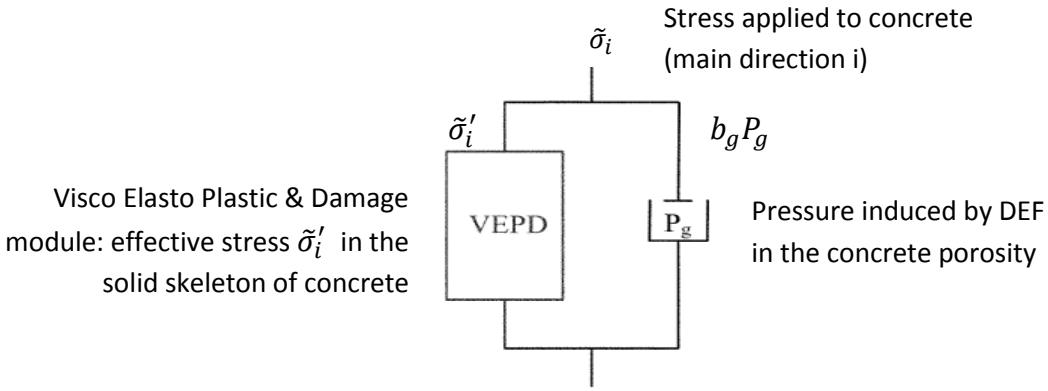

Figure 10 : Idealized scheme of the poro-mechanical model of concrete affected by DEF

$$\begin{cases} \sigma_i = (1 - D_i)\tilde{\sigma}_i \\ \tilde{\sigma}_i = \tilde{\sigma}_i' - b_g P_g \end{cases} \quad (33)$$

with b_g the Biot coefficient for the DEF and P_g the pressure due to DEF.

In equation (33), σ_i is the main stress, D_i is the damage induced in the main direction "i" by swelling and external loading in the solid skeleton of the concrete, $\tilde{\sigma}_i$ is the total stress in the undamaged part of the concrete (stress in the matrix plus stress due to the DEF pressure), $\tilde{\sigma}_i'$ is the effective stress in the undamaged part of the concrete (depending only on the elastic strain in the matrix according to equation 34):

$$\begin{cases} \tilde{\sigma}_i' = \lambda^{tr}\bar{\bar{\varepsilon}}^e + 2\mu\varepsilon_i^e \\ \bar{\bar{\varepsilon}}^e = \bar{\bar{\varepsilon}} - \bar{\bar{\varepsilon}}^c - \bar{\bar{\varepsilon}}^{p,m} - \bar{\bar{\varepsilon}}^{p,g} \end{cases} \quad (34)$$

with λ and μ the Lamé elastic coefficients of undamaged concrete, $\bar{\bar{\varepsilon}}$ the mechanical strain tensor (total strain minus thermal strain), $\bar{\bar{\varepsilon}}^c$ the creep strain tensor computed according to the model presented in [41], $\bar{\bar{\varepsilon}}^{p,m}$ the plastic strains associated with the cracking induced by the external loading and computed according to the model presented in [39]. $\bar{\bar{\varepsilon}}^{p,g}$ is the irreversible strain induced by the DEF and computed as explained below. Note that the creep and irreversible strains are combined in equation (34) to compute the effective stress in the concrete matrix ($\tilde{\sigma}_i'$), then equation (33) allows the resulting stress (σ_i) to be assessed, which also takes the effect of pressure P_g induced by the DEF and the effect of cracking on concrete stiffness into consideration through the damage variable D_i. Therefore, the main benefit of the poro-mechanical formulation is to combine all the non-linear phenomena involved in the long-term behaviour of concrete in a relatively simple formulation. The benefits of a poro-mechanical formulation have already been underlined by other authors [12,46].

In the current work, the model directly uses the volume of ettringite supplied by the chemical equations presented above to compute a pore pressure given by equation (35):

$$P_g = M_g\left(\emptyset_{DEF} - \left(\frac{\emptyset_{DEF}^v C_g P_g}{R_t} + b_g{}^{tr}(\bar{\bar{\varepsilon}}^e + \bar{\bar{\varepsilon}}^c + \bar{\bar{\varepsilon}}^{p,m}) + {}^{tr}\bar{\bar{\varepsilon}}^{p,g}\right)\right) \quad (35)$$

In equation (35), M_g is the Biot modulus controlling the mechanical interaction between the delayed ettringite volume $\emptyset_{DEF}$ (compressibility modulus K_g) and the surrounding matrix (compressibility modulus K_m). The Biot modulus can be assessed using equation (36):

$$\frac{1}{M_g} = \frac{b_g - \emptyset_{DEF}}{K_m} + \frac{\emptyset_{DEF}}{K_g} \quad (36)$$

In which the Biot coefficient b_g can be assessed with equation (37) if a Mori Tanaka scheme of homogenization [32] is used with a Poisson coefficient of the matrix of 0.2 :

$$b_g = \frac{2\emptyset_{DEF}}{1+\emptyset_{DEF}} \quad (37)$$

In the Mori Tanaka method, $\emptyset_{DEF}$ represents the volume of void filled by the fluid with the pressure Pg. If this pressure is equal to the crystallization pressure, as the crystallisation takes place in water K_g is equal to 2.1 GPa. In (36), K_m is the compressibility modulus of the matrix around the void filled by the water under pressure P_g, it can be deduced of the concrete compressibility coefficient K_c using equation (38).

$$K_m = \frac{K_c}{1-b_g} \quad (38)$$

Considering these assumptions, the Biot coefficient and modulus vary during the reaction due to the variation of the volume of ettringite $\emptyset_{DEF}$ given by equation (39), based on the chemical variables supplied by equations (17) or (18):

$$\frac{\partial \emptyset_{\mathrm{DEF}}}{\partial \mathrm{t}} = \mathrm{V_{AFt}} \frac{\partial \mathrm{E_2}}{\partial \mathrm{t}} - \mathrm{V_{AFm}} \frac{\partial \mathrm{M_1}}{\partial \mathrm{t}} \quad (39)$$

with $V_{AFt} = 715\ cm^3/mol$ and $V_{AFm} = 254\ cm^3/mol$ according to [1] who cites [20], the molar volumes of ettringite and mono-sulfates. According to [45] part of the monosulfate can be replaced by DEF in certain situations as explained in the presentation of the chemical model. In equation (35), $\emptyset_{DEF}^{v}$ is the volume to be filled, in a specimen free of stresses, around the sites of DEF before the pressure damages the concrete matrix [19], this volume leads to a reduction of swelling for small values of $\emptyset_{DEF}$, compensating the overestimation of small swelling pointed out in Figure 6 for the chemical model used alone. R_t is the tensile strength of concrete, Cg the stress concentration factor.

In equations (34) and (35), $\bar{\bar{\varepsilon}}^{p,g}$ is the plastic strain, which represents the irreversible diffuse cracking induced in the solid skeleton (left branch in Figure 10) by the pressure when its combination with external loading ($\tilde{\sigma}_i$) exceeds the tensile strength (R_t) of the concrete matrix. The plastic criterion driving this diffuse cracking due to pressure between cement paste and aggregates can be assessed in each main direction "i" of stresses:

$$f(P_g, \tilde{\sigma}_i) = \begin{cases} C_g P_g + \tilde{\sigma}_i - R_t & if\ \tilde{\sigma}_i < R_t \\ P_g & if\ \tilde{\sigma}_i \geq R_t \end{cases} \quad (40)$$

With C_g the stress concentration factor around aggregates taken to one for sake of simplicity (spherical inclusions in a swelling matrix). For the stress state in the concrete matrix ($\tilde{\sigma}_i' \leq R_t$) to be

considered admissible, $f(P_g, \tilde{\sigma}_i)$ has to stay lower than zero. It then controls the evolution of plastic strain $\bar{\varepsilon}^{p,g}$ according to the consistency conditions of plasticity: as soon as a pressure P_g leads to the criterion (equation 37) being exceeded, a plastic increment $d\varepsilon_i^{p,g}$ is computed to return the yield function $f(P_g, \tilde{\sigma}_i)$ to zero (equation's set 40):

$$\begin{cases} \left(\frac{\partial f}{\partial P_g} \frac{\partial P_g}{\partial \varepsilon_i^{p,g}} + \frac{\partial f}{\partial \tilde{\sigma}_j} \frac{\partial \tilde{\sigma}_j}{\partial \tilde{\sigma}_k'} \frac{\partial \tilde{\sigma}_k'}{\partial \varepsilon_i^{p,g}} + \frac{\partial f}{\partial R_t} \frac{\partial R_t}{\partial \varepsilon_i^{p,g}} \right) d\varepsilon_i^{p,g} + f(P_g, \tilde{\sigma}_i) = 0 \\ d\varepsilon_i^{p,g} = d\lambda_i \frac{\partial f}{\partial \tilde{\sigma}_i} \end{cases} \quad (41)$$

In (41) $d\lambda_i$ is a plastic multiplier adjusted to verify the first equation in (40). Note that, through the formulation of (40), an external loading corresponding to a compression ($\tilde{\sigma}_i \leq 0$) reduces the yield function $f(P_g, \tilde{\sigma}_i)$, and then delays or prevents swelling in the corresponding direction. Consequently, the pressure can increase in the matrix until the criterion is exceeded in another direction. This formulation is thus able to model anisotropic swelling induced by the interaction between the pressure induced by ettringite precipitation and non-isotropic external loading as observed in [3]. The ability of this plastic criterion to manage anisotropic swelling has been confirmed, for instance for a pressure induced by alkali-aggregate reaction [31]. Once the plastic strain tensor has been updated with the increments (41), its main values are computed and used to assess the corresponding damage variables, which take the reduction of concrete stiffness induced by micro-cracking (equation 42) into account:

$$d_i = \frac{\varepsilon_i^{p,g}}{\varepsilon_0 + \varepsilon_i^{p,g}} \quad (42)$$

The damage then affects the Young modulus of the matrix through the equations (33-34), thus considering the damage due to the swelling (43).

$$D_i = \begin{cases} 1 - \left((1 - d_j)(1 - d_k) \right)^{\alpha}, & \tilde{\sigma}_i < 0 \\ d_i, & \tilde{\sigma}_i \geq 0 \end{cases} \quad (43)$$

In equation (43) (d_i, d_j, d_k) are the main values of the damage induced by the DEF (equation 43 applied in the three main directions of $\bar{\varepsilon}^{p,g}$), $\alpha \approx 0.15$ according to [40], considers that micro-cracking is less efficient to reduce the concrete stiffness in compression than in tension due to the possible re-closure under compression of some micro-cracks filled by ettringite.

In equation (42), $\varepsilon_0 \approx 0.3\%$ is a constant to link the plastic strain and the tensile damage due to the matrix micro-cracking. α and ε_0 were first used in 2002 for AAR modelling by [9]. The first calculations for DEF are performed with the same data as for alkali-aggregate reaction but future

uses of this model to simulate other configurations [3,30] will confirm the parameters or will lead to modifications of some of them.

3.2 Application to the alkali leaching effect on expansion (analysis of Martin's results)

The case considered here is a cylindrical specimen studied by Martin [29]. The main material characteristics are given in Table 3, they are close to the Kchakech's sones [26]. The temperature chronology, including the heating period, is presented in Figure 11. Figure 12 provides a zoom to show the details of the heating cycle. As the specimen is stored in tap water, alkali leaching occurs during the storage. This leaching is considered using a diffusion equation of alkali in the saturated porosity of the specimen, and a boundary condition for the surfaces in contact with the external water (Na = 0 mol/l in equation 44 is an approximation of tap water by pure water for sake of simplicity). As the specimen and the boundary conditions present cylindrical symmetry, the finite element model is meshed in an axisymmetric base, and only the upper half of the specimen is modelled.

$$\begin{cases} (\phi + k.CSH)\frac{\partial(Na)}{\partial t} = div\left(D_{Na}\overrightarrow{grad}(Na)\right), \forall M \in \Omega \\ Na(M, t=0) = 0.91\frac{mol}{l}, \forall M \in \Omega \\ Na(M,t) = 0.\frac{mol}{l}, \forall t, \forall M \in \delta\Omega \end{cases} \quad (44)$$

In (43), M is any point in Ω, the volume of the specimen, and $\delta\Omega$ is its boundary in contact with the water of the storage bath. The initial condition Na=0.91 mol/l corresponds to the data in the last line of Table 3.

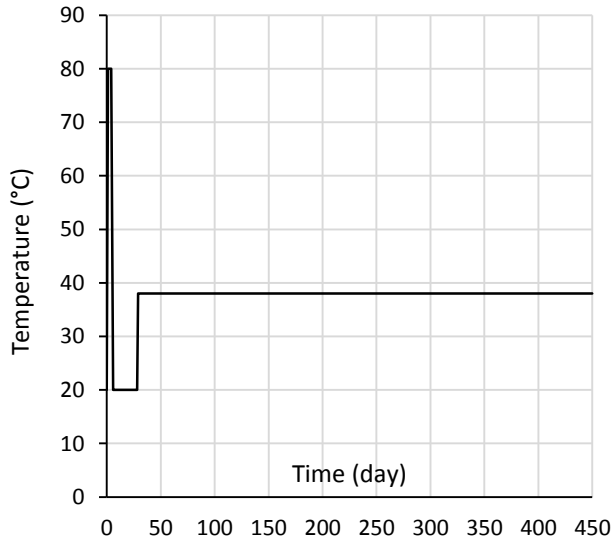

Figure 11: Thermal cycle (72h at 80°C, aging at 38°C after 28 days)

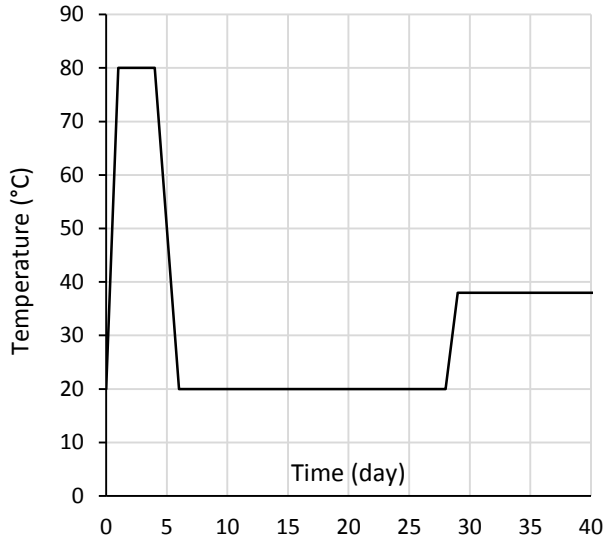

Figure 12 : Thermal cycle, zoom on first 50 days

An illustration of the alkali concentration in the pores of the concrete is supplied in Figure 13, where the ratio of residual alkali to initial alkali is given versus time (a) with a concentration field at the end of the simulation (b). In Figure 13(a), the two crosses correspond to measurements performed by Martin. The diffusion coefficient, $D_{Na} \approx 0.5\ 10^{-12}\ s^{-1}$, was fitted to reproduce the leaching kinetics.

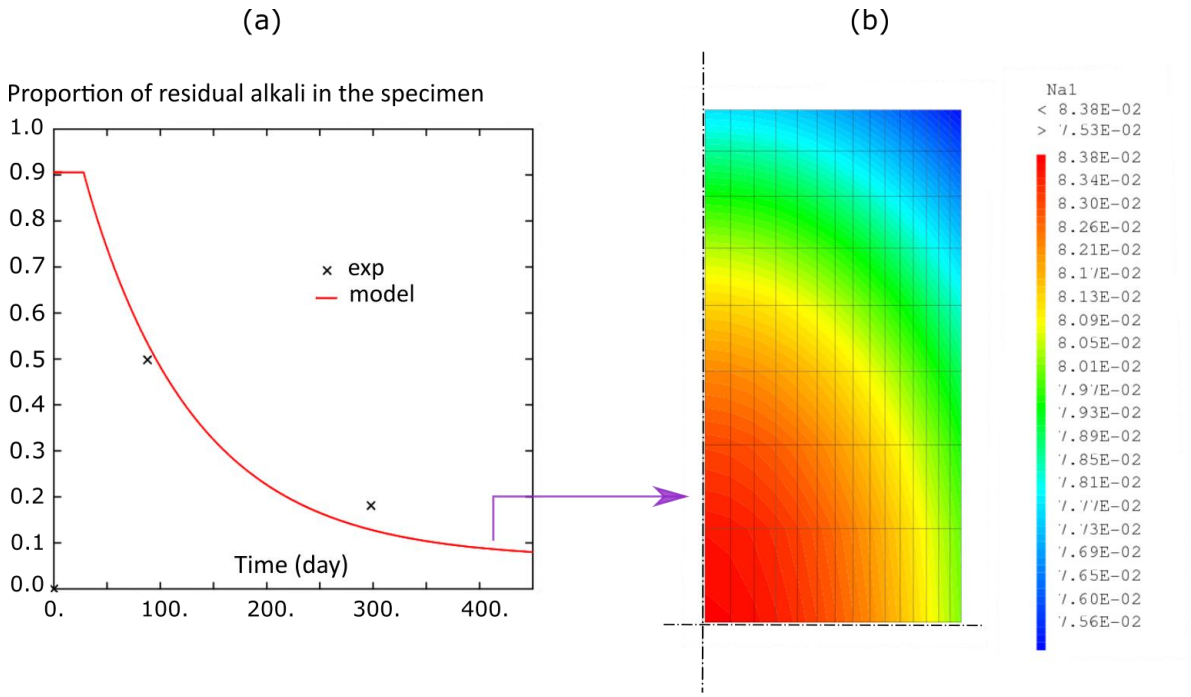

Figure 13: Proportion of residual alkali in the specimen versus time (a), final alkali concentration plotted on the axisymmetric mesh of the half upper part of the specimen (b)

Once the alkali concentration is known for each time step of the stepwise analysis, the chemical model and the poro-mechanical models described above can be used. Figure 14 (a) shows the evolution of the state variables of the chemical model during the test. The production of secondary Aft (AFT2 in the graph legend corresponding to E2 in the chemical equations) increases between 50 and 200 days, and the available sulfates ($STIL = \tilde{S}$) and aluminates (ATIL=$\tilde{A}$) decrease simultaneously. The DEF stops after around 200 days due to lack of sulfates ($STIL = 0$). Figure 14(b) gives an illustration of the variable VAFT corresponding to $\emptyset_{DEF}$ in equations (35) and (36), plotted on the deformed mesh (amplified 100 times). The deformed mesh shows that swelling is faster in the upper right corner of the specimen due the faster alkali leaching in this zone; which accelerates the DEF as illustrated in Figure 4.

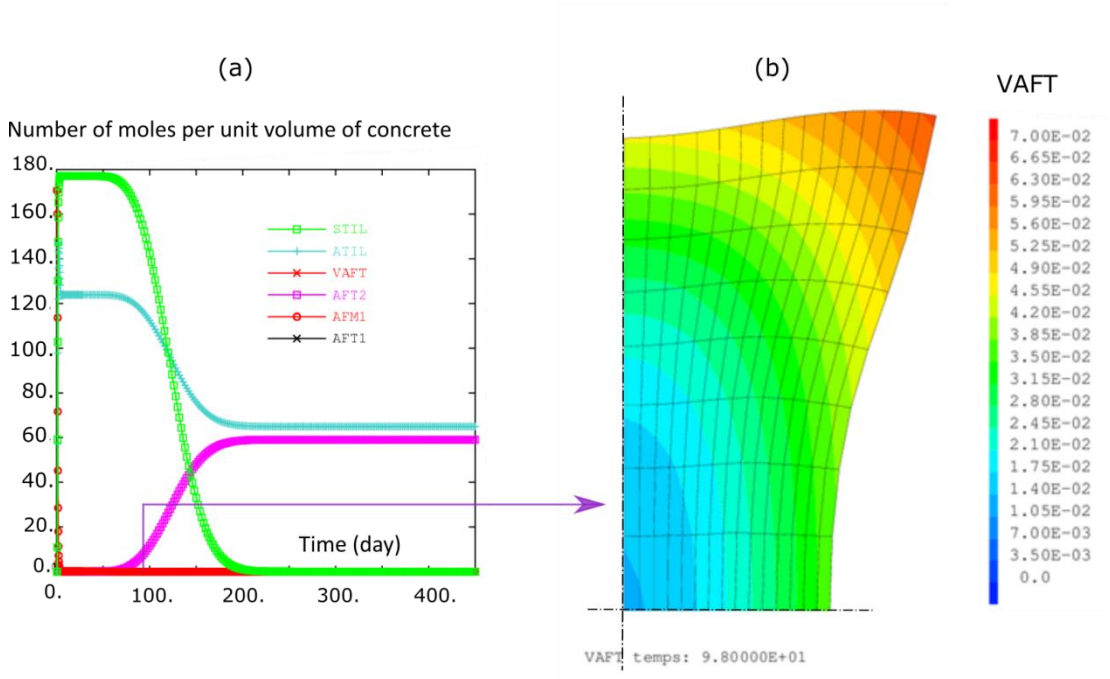

Figure 14: Chemical species evolution versus time at the centre of the specimen (a), Effective Volume of DEF at 100 days on deformed mesh (displacement x100) (b)

Figure 15 is a zoom of Figure 14(a) for the first 7 days. During the temperature plateau at 80°C, the number of moles of primary AFm (AFM1 in Figure 15) decreases in favour of available sulfates (STIL) and aluminates (ATIL). From day two, the available aluminate starts to decrease due to the formation of hydrogarnet, which occurs while the temperature exceeds $T_{th,f}$ =70°C. Afterwards, the evolutions stop because the temperature passes below the threshold value ($T_{th,d}$), and the alkali content in the specimen is still too high for DEF. DEF occurs later as illustrated in Figure 14, with alkali leaching.

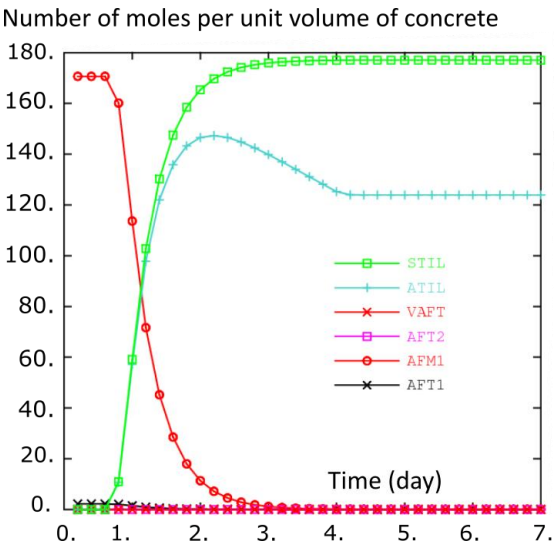

662

663 **Figure 15: Chemical concentration versus time (zoom on first 7 days including heating period)**

664 Figure 16 (a) shows the swelling versus time computed by the model (lines), compared with
665 experimental swelling (crosses). Each coloured line represents the swelling direction (radial direction
666 in red and vertical in green and blue) and location (in core in blue and along external surface in
667 green) given on the mesh (b). The swelling starts at the upper right corner (green line in (a) starts
668 first; it corresponds to the green arrow swelling in (b)).

669

(a) (b)

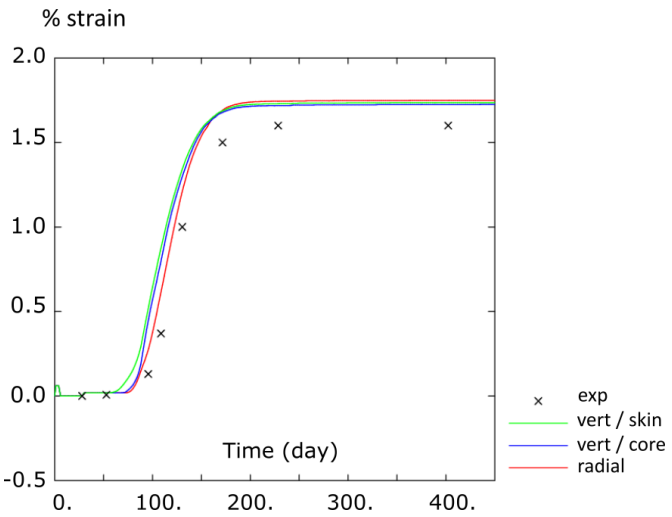

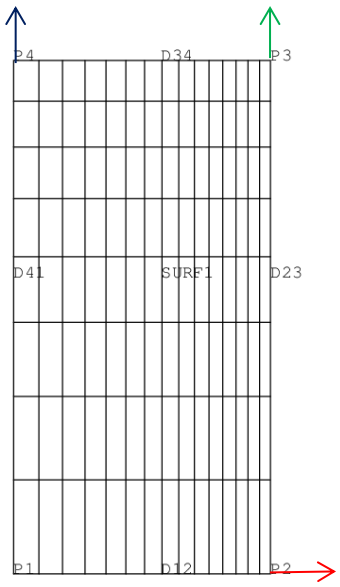

Finite elements mesh (1/4 of the specimen)

670 **Figure 16 : Simulated Swelling strain at different points versus time compared to experimental results of Martin's tests**
671 [29]

Figure 17 illustrates the stress state computed by the poro-mechanical model at 100 days. As the model used is based on linear interpolation functions in the finite elements for the displacements fields, the stresses appear quite discontinuous, this is a numerical artefact induced by the great gradient of swelling in this zone at this stage. However, their magnitudes remain correct, because they correspond to the better approximation allowed by the weak form of the variationnal principle applied to the equilibrium equation, with an admissible relative accuracy of 5.e-4. At this stage, the swelling is more developed close to the surface of the specimen than at its centre. Consequently, compressive stresses appear near the surface (blue zones), while the core of the specimen is in tension. This stress state evolves during the DEF and, at the end of the test, the stress state reverses and the edges in contact with water crack. Figure 18 gives the damage and localized cracks opening predicted by the model. The crack pattern at 100 days (c) is compared to a picture from Kchakech PhD thesis [26] (b) in which the same concrete than in Martin's work is used. Experimentally localized and diffuse cracking coexist. The model is able to distinguish cracks due to local swelling to cracks due to the swelling gradients. The diffuse damage is mainly due to the internal pressure of DEF, while localized cracks are induced by the gradient of swelling, they are the "structural" cracks and appear progressively between the swelling zone and the core of the specimen as illustrated in Figure 18 (d). After 100 days most of the localized cracks are developed and do not evolve anymore until the end of the test because the swelling becomes quasi-homogenous over the specimen after this date.

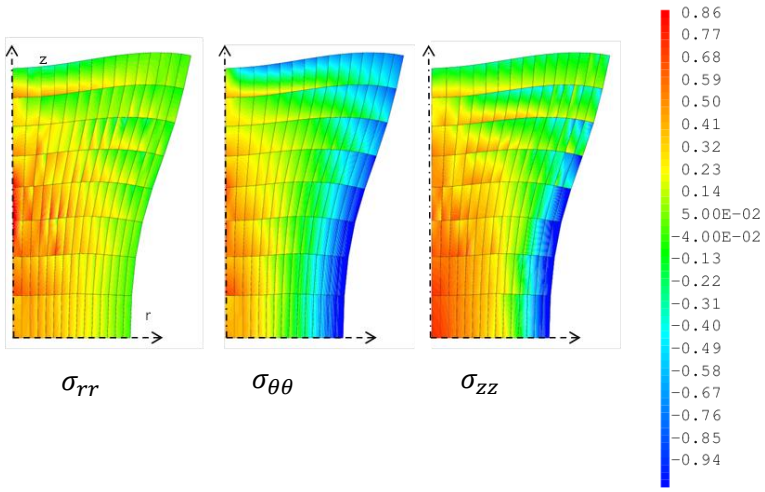

Figure 17: Simulation of Stress state (MPa) during swelling of Martin's tests [29] (at 100 days, deformed mesh X 100)

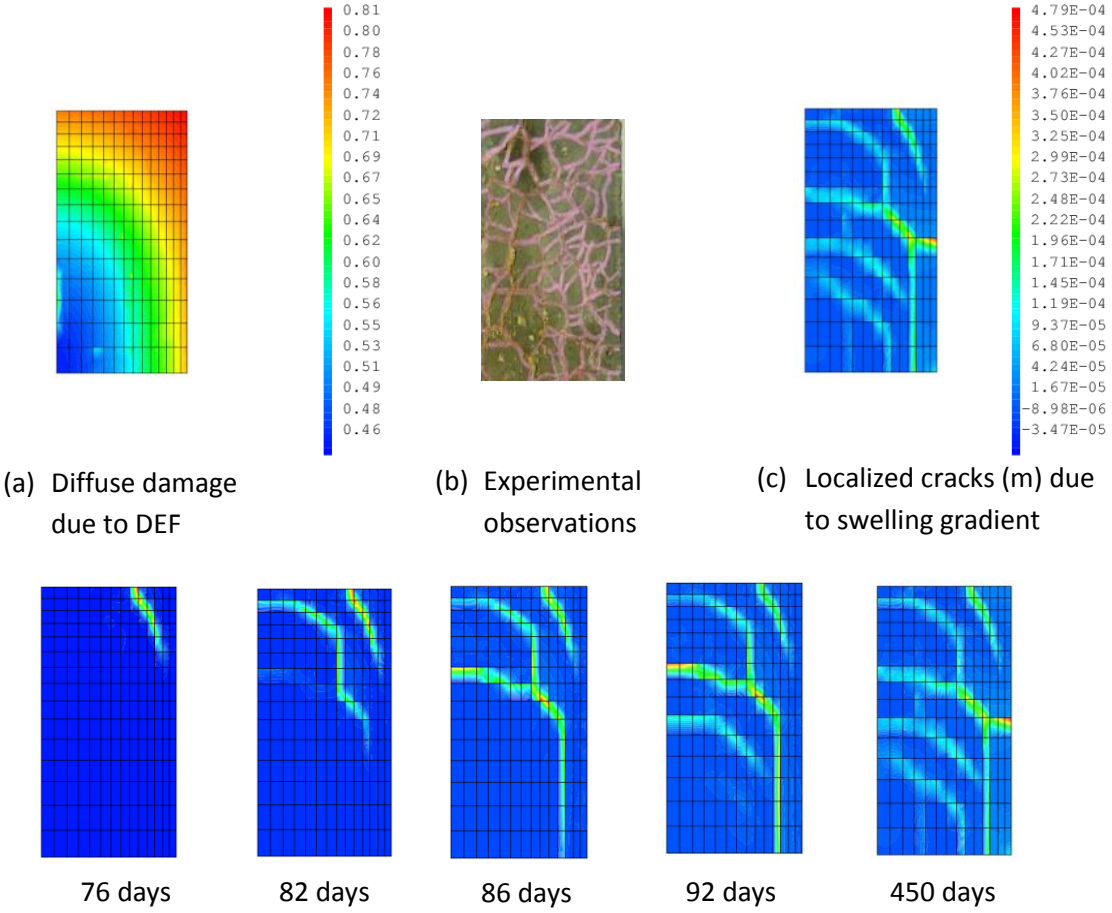

Figure 18 : Damage pattern predicted by the model compared to the cracking pattern of Kchakech's specimen at 100 days (same concrete and process than Martin [29]). (a) Diffuse damage due to the DEF pressure : scale 0 undamaged to 1 damaged (b) picture from Kchakech PhD thesis [26](c) localized cracks predicted by the model

4 Conclusion

A chemical model has been proposed for the study of structures affected by DEF. It considers the dissolution of primary sulfoaluminate hydrates and the possible fixation of aluminates during hot periods, which explains the pessimum effect of heating duration observed in several experiments. The model gives importance to the role of alkali, which affects the threshold temperature of dissolution, the kinetics of dissolution, the thermal conditions and kinetics of aluminates fixation at high temperature. At low temperature, alkalis can delay or prevent DEF according to their concentration. At low temperature, the chemical model considers that DEF can be due either to the conversion of monosulfate into trisulfoaluminates or due directly to the formation of Aft from available sulfates and aluminates reversibly stored in C-S-H. The model was fitted with different materials, heating cycles and storage conditions. It is able to explain the swelling potential of various laboratory tests with a determination coefficient R^2 of 90%, using a single set of parameters. The

main result of the chemical model is the number of moles of ettringite, which can be used in a poro-mechanical model through the pressure induced by DEF in the pores of the concrete. The structural effects of DEF can thus be assessed: in particular the swelling, the damage induced by DEF, and the localized cracks induced by swelling gradients. If the pressure, combined with the external loading, is great enough to provoke cracking, diffuse damage appears, reducing the strength of the concrete, occurring differently in tension and in compression. The model has been implemented in a finite element code and tested for the simulation of different basic experiments taken from a literature review. Now the model should be applied to larger and more sophisticated structures in order to validate or to improve the mechanical formulation. Forthcoming work will concern, in particular, the modelling of beams studied at IFSTTAR, Paris, by R.P. Martin, as these beams present different reinforcement rates and should thus allow the fitting of the mechanical part of the model to be refined.

5 Acknowledgements

The authors thank the C.E.A (French Atomic and Alternative Energy Center) for the supply of finite element software Castem in its research and development version [8].

Appendix: Evolution of state variables during a temperature plateau T>T_{th}

For a cement with an amountA_c of aluminate and with the initial conditions given at $t = t_0$:

$$\begin{cases} \tilde{A}(t_0) = \tilde{A}_0 \\ \tilde{S}(t_0) = \tilde{S}_0 \\ M_1(t_0) = M_{1,0} \\ E_1(t_0) = E_{1,0} \\ E_2(t_0) = E_{2,0} \end{cases}$$

if the ratio $\tau_d/\tau_f > 1$ and T>$T_{th,f}$, the evolution of $\tilde{A}$ is given by:

$$\tilde{A} = \tilde{A}_0 exp\left(-\frac{t-t_0}{\tau_f}\right) + \left(M_{1,0} + E_{1,0} + E_{2,0}\right)\left(\frac{\tau_f/\tau_d}{\tau_f/\tau_d - 1}\right)\left(exp\left(-\frac{t-t_0}{\tau_f}\right) - exp\left(-\frac{t-t_0}{\tau_d}\right)\right)$$

and the evolution of $\tilde{S}$ by:

$$\tilde{S} = \tilde{S}_0 + \left(M_{1,0} + 3\left(E_{1,0} + E_{2,0}\right)\right)\left(1 - exp\left(-\frac{t-t_0}{\tau_d}\right)\right)$$

The hydrate amounts during the hot period then evolve as follows:

733 $$\begin{cases} M_1 = M_{1,0} exp\left(-\frac{t-t_0}{\tau_d}\right) \\ E_1 = E_{1,0} exp\left(-\frac{t-t_0}{\tau_d}\right) \\ E_2 = E_{2,0} exp\left(-\frac{t-t_0}{\tau_d}\right) \end{cases}$$

734 # References

735 [1] F. Adenot, «Durabilité du béton: caractérisation et modélisation des processus physiques et
736 chimiques de dégradation du ciment», Université d'Orléans, 1992.

737 [2] B. Bary, N. Leterrier, E. Deville, P. Le Bescop, Coupled chemo-transport-mechanical modelling
738 and numerical simulation of external sulfate attack in mortar, Cem. Concr. Compos. 49 (2014)
739 70–83.

740 [3] H. Bouzabata, S. Multon, A. Sellier, H. Houari, Effects of restraint on expansion due to delayed
741 ettringite formation, Cem. Concr. Res. 42 (2012) 1024–1031.

742 [4] X. Brunetaud, Etude de l'influence de différents paramètres et de leurs interactions sur la
743 cinétique et l'amplitude de la réaction sulfatique interne au béton, Ph.D. thesis, Laboratoire
744 Central des Ponts et Chaussées., 2005.

745 [5] X. Brunetaud, R. Linder, L. Divet, D. Duragrin, D. Damidot, Effect of curing conditions and
746 concrete mix design on the expansion generated by delayed ettringite formation, Mater.
747 Struct. 40 (2007) 567–578.

748 [6] L. Buffo-Lacarriére, A. Sellier, Chemo-mechanical modeling requirements for the assessment
749 of concrete structure service life, J. Eng. Mech. 137 (2011).

750 [7] L. Buffo-Lacarrière, A. Sellier, G. Escadeillas, A. Turatsinze, Multiphasic finite element
751 modeling of concrete hydration, Cem. Concr. Res. 37 (2007) 131–138.

752 [8] C.E.A, Cast3M 2017 Finite Element Software, (2017).

753 [9] B. Capra, A. Sellier, Orthotropic modelling of alkali-aggregate reaction in concrete structures :
754 numerical simulations, Mech. Mater. 6 (2002).

755 [10] C. Comi, R. Fedele, U. Perego, A chemo-thermo-damage model for the analysis of concrete
756 dams affected by alkali-silica reaction, Mech. Mater. 41 (2009) 210–230.

757 [11] C.W. Correns, Growth and dissolution of crystals under linear pressure, Discuss. Faraday Soc.
758 5 (1949) 267.

759 [12] O. Coussy, P. Monteiro, Unsaturated poroelasticity for crystallization in pores, Comput.
760 Geotech. 34 (2007) 279–290.

761 [13] D. Damidot, F.P. Glasser, Thermodynamic investigation of the CaO Al2O3 CaSO4 H2O system
762 at 50°C and 85°C, Cem. Concr. Res. 22 (1992) 1179–1191.

763 [14] D. Damidot, F.P. Glasser, Thermodynamic investigation of the CaO Al2O3 CaSO4 H2O system
764 at 25°C and the influence of Na2O, Cem. Concr. Res. 23 (1993) 221–238.

765 [15] D. Damidot, S. Stronach, A. Kindness, M. Atkins, F.P. Glasser, Thermodynamic investigation of
766 the CaO Al2O3 CaCO3 H2O closed system at 25°C and the influence of Na2O, Cem. Concr. Res.
767 24 (1994) 563–572.

768 [16] B.Z. Dilnesa, B. Lothenbach, G. Renaudin, A. Wichser, D. Kulik, Synthesis and characterization
769 of hydrogarnet Ca3(AlxFe1−x)2(SiO4)y(OH)4(3−y), Cem. Concr. Res. 59 (2014) 96–111.

770 [17] L. Divet, R. Randriambololona, Delayed Ettringite Formation: The Effect of Temperature and
771 Basicity on the Interaction of Sulphate and C-S-H Phase, Cem. Concr. Res. 28 (1998) 357–363.

772 [18] C. Famy, K.. Scrivener, A. Atkinson, A.. Brough, Influence of the storage conditions on the
773 dimensional changes of heat-cured mortars, Cem. Concr. Res. 31 (2001) 795–803.

774 [19] R.J. Flatt, G.W. Scherer, Thermodynamics of crystallization stresses in DEF, Cem. Concr. Res.
775 38 (2008) 325–336.

776 [20] Frederick M. Lea;C.H. Desch:, The Chemistry of Cement and Concrete, 1970.

777 [21] B. Godart, L. Divet, The new french recommendations to prevent disorders due to delayed
778 ettringite formation, HAL CCSD, 2008.

779 [22] E. Grimal, A. Sellier, S. Multon, Y. Le Pape, E. Bourdarot, Concrete modelling for expertise of
780 structures affected by alkali aggregate reaction, Cem. Concr. Res. 40 (2010) 502–507.

781 [23] E. Grimal, A. Sellier, Y. Le Pape, E. Bourdarot, Creep, Shrinkage, and Anisotropic Damage in
782 Alkali-Aggregate Reaction Swelling Mechanism-Part I. A Constitutive Model, ACI Mater. J. 105
783 (2008) 227–235.

784 [24] S.-Y. Hong, F.P. Glasser, Alkali binding in cement pastes: Part I. The C-S-H phase, Cem. Concr.
785 Res. 29 (1999) 1893–1903.

786 [25] M.M. Karthik, J.B. Mander, S. Hurlebaus, ASR/DEF related expansion in structural concrete:

787 Model development and validation, Constr. Build. Mater. 128 (2016) 238–247.

788 [26] B. Kchakech, Etude de l'influence de l'échauffement subi par un béton sur le risque
789 d'expansions associées à la Réaction Sulfatique Interne, Paris Est, 2015.

790 [27] T. De Larrard, F. Benboudjema, J.B. Colliat, J.M. Torrenti, F. Deleruyelle, Concrete calcium
791 leaching at variable temperature: Experimental data and numerical model inverse
792 identification, Comput. Mater. Sci. 49 (2010) 35–45.

793 [28] LCPC, Guide méthodologique : Aide à la gestion des ouvrages atteints de réactions de
794 gonflement interne, 2003.

795 [29] R.-P. Martin, Analyse sur structures modèles des effets mécaniques de la réaction sulfatique
796 interne du béton, Paris Est, 2010.

797 [30] R.-P. Martin, D. Siegert, F. Toutlemonde, Experimental analysis of concrete structures
798 affected by DEF: Influence of moisture and restraint, in: Thermo-Hydromechanical Chem.
799 Coupling Geomaterials Appl., France, 2008: pp. 334–340.

800 [31] P. Morenon, S. Multon, A. Sellier, E. Grimal, F. Hamon, E. Bourdarot, Impact of stresses and
801 restraints on ASR expansion, Constr. Build. Mater. 140 (2017) 58–74.

802 [32] T. Mori, K. Tanaka, Average stress in matrix and average elastic energy of materials with
803 misfitting inclusions, Acta Metall. 21 (1973) 571–574.

804 [33] G. Möschner, B. Lothenbach, F. Winnefeld, A. Ulrich, R. Figi, R. Kretzschmar, Solid solution
805 between Al-ettringite and Fe-ettringite, Cem. Concr. Res. 39 (2009) 482–489.

806 [34] A. Pavoine, X. Brunetaud, L. Divet, The impact of cement parameters on Delayed Ettringite
807 Formation, Cem. Concr. Compos. (2011).

808 [35] S. Poyet, A. Sellier, G. Foray, H. Cognon, E. Bourdarot, A.A. Sellier, et al., Chemical modelling
809 of Alkali Silica reaction: Influence of the reactive aggregate size distribution, Mater. Struct. 40
810 (2007) 229–239.

811 [36] M. Salgues, A. Sellier, S. Multon, E. Bourdarot, E. Grimal, DEF modelling based on
812 thermodynamic equilibria and ionic transfers for structural analysis, Eur. J. Environ. Civ. Eng.
813 (2014) 1–26.

814 [37] V. Saouma, L. Perotti, Constitutive model for alkali-aggregate reactions, ACI Mater. J. 103
815 (2006) 194.

[38] J.-F. Seignol, N. Baghdadi, F. Toutlemonde, A macroscopic chemo - mechanical model aimed at reassessment of delayed - ettringite - formation affected concrete structures, in: M. Fischinger (Ed.), Proc. First Int. Conf. Comput. Technol. Concr. Struct. (CTCS 09), 24-27 May 2009, Jeju, Korea Vol. Keynote Pap. Abstr. with Full Texts Pap. a CD-ROM, 2009: pp. 1–19.

[39] A. Sellier, Model FLUENDO3D Version 20-P for Castem 2012, Handbook, LMDC Internal Document., Toulouse, 2015.

[40] A. Sellier, B. Bary, Coupled damage tensors and weakest link theory for the description of crack induced anisotropy in concrete, 69 (2002) 1925–1939.

[41] A. Sellier, S. Multon, L. Buffo-lacarrière, T. Vidal, X. Bourbon, G. Camps, Concrete creep modelling for structural applications : non-linearity , multi-axiality , hydration , temperature and drying effects, Cem. Concr. Res. 79 (2016) 301–315.

[42] M. Al Shamaa, S. Lavaud, L. Divet, J.B. Colliat, G. Nahas, J.M. Torrenti, Influence of limestone filler and of the size of the aggregates on DEF, Cem. Concr. Compos. 71 (2016) 175–180.

[43] M. Al Shamaa, S. Lavaud, L. Divet, G. Nahas, J.M. Torrenti, Coupling between mechanical and transfer properties and expansion due to DEF in a concrete of a nuclear power plant, Nucl. Eng. Des. 266 (2014) 70–77.

[44] M. Al Shamaa, S. Lavaud, L. Divet, G. Nahas, J.M. Torrenti, Influence of relative humidity on delayed ettringite formation, Cem. Concr. Compos. 58 (2015) 14–22.

[45] H.F.. Taylor, C. Famy, K.. Scrivener, Delayed ettringite formation, Cem. Concr. Res. 31 (2001) 683–693.

[46] F.-J. Ulm, O. Coussy, K. Li, C. Larive, Thermo-Chemo-Mechanics of ASR expansion in concrete structures, ASCE J. Eng. Mech. 126 (2000) 233–242.